

000 054  
 001 055  
 002 056  
 003 057  
 004 058  
 005 059  
 006 060  
 007 061  
 008 062  
 009 063  
 010 064  
 011 065  
 012 066  
 013 067  
 014 068  
 015 069  
 016 070  
 017 071  
 018 072  
 019 073  
 020 074  
 021 075  
 022 076  
 023 077  
 024 078  
 025 079  
 026 080  
 027 081  
 028 082  
 029 083  
 030 084  
 031 085  
 032 086  
 033 087  
 034 088  
 035 089  
 036 090  
 037 091  
 038 092  
 039 093  
 040 094  
 041 095  
 042 096  
 043 097  
 044 098  
 045 099  
 046 100  
 047 101  
 048 102  
 049 103  
 050 104  
 051 105  
 052 106  
 053 107

## Supplementary Material to “External Prior Guided Internal Prior Learning for Real Noisy Image Denoising”

Anonymous CVPR submission

Paper ID 1047

In this supplementary material, we provide:

1. The closed-form solution of the sparse coding problem (6) in the main paper.
2. More denoising results on the real noisy images in dataset [1].
3. More results on the 15 cropped real noisy images (with mean image of 500 shots as “ground truth”) in dataset [2].
4. More results on the 60 cropped real noisy images (with mean image of 500 shots as “ground truth”) in dataset [2].

### 1. Closed-Form Solution of the Weighted Sparse Coding Problem (6)

For notation simplicity, we ignore the indices  $n, m, t$  in problem (6) of the main paper. It turns into the following weighted sparse coding problem:

$$\min_{\alpha} \|\mathbf{y} - \mathbf{D}\alpha\|_2^2 + \sum_{j=1}^{3p^2} \lambda_j |\alpha_j|. \quad (1)$$

Since  $\mathbf{D}$  is an orthogonal matrix, problem (1) is equivalent to

$$\min_{\alpha} \|\mathbf{D}^T \mathbf{y} - \alpha\|_2^2 + \sum_{j=1}^{3p^2} \lambda_j |\alpha_j|. \quad (2)$$

For simplicity, we denote  $\mathbf{z} = \mathbf{D}^T \mathbf{y}$ . Here we have  $\lambda_j > 0, j = 1, \dots, 3p^2$ , then problem (2) can be written as:

$$\min_{\alpha} \sum_{j=1}^{3p^2} ((\mathbf{z}_j - \alpha_j)^2 + \lambda_j |\alpha_j|). \quad (3)$$

The problem (3) is separable w.r.t. each  $\alpha_j$  and hence can be simplified to  $3p^2$  independent scalar minimization problems

$$\min_{\alpha_j} (\mathbf{z}_j - \alpha_j)^2 + \lambda_j |\alpha_j|, \quad (4)$$

where  $j = 1, \dots, 3p^2$ . Taking derivative of  $\alpha_j$  in problem (4) and setting the derivative to be zero. There are two cases for the solution.

(a) If  $\alpha_j \geq 0$ , we have

$$2(\alpha_j - \mathbf{z}_j) + \lambda_j = 0. \quad (5)$$

The solution is

$$\hat{\alpha}_j = \mathbf{z}_j - \frac{\lambda_j}{2} \geq 0. \quad (6)$$

So  $\mathbf{z}_j \geq \frac{\lambda_j}{2} > 0$ , and the solution  $\hat{\alpha}_j$  can be written as

$$\hat{\alpha}_j = \text{sgn}(\mathbf{z}_j) * (|\mathbf{z}_j| - \frac{\lambda_j}{2}), \quad (7)$$

where  $\text{sgn}(\bullet)$  is the sign function.

(b) If  $\alpha_j < 0$ , we have

$$2(\alpha_j - \mathbf{z}_j) - \lambda_j = 0. \quad (8)$$

The solution is

$$\hat{\alpha}_j = \mathbf{z}_j + \frac{\lambda_j}{2} < 0. \quad (9)$$

108 So  $\mathbf{z}_j < -\frac{\lambda_j}{2} < 0$ , and the solution  $\hat{\alpha}_j$  can be written as  
 109

$$\hat{\alpha}_j = \text{sgn}(\mathbf{z}_j) * (-\mathbf{z}_j - \frac{\lambda_j}{2}) = \text{sgn}(\mathbf{z}_j) * (|\mathbf{z}_j| - \frac{\lambda_j}{2}). \quad (10)$$

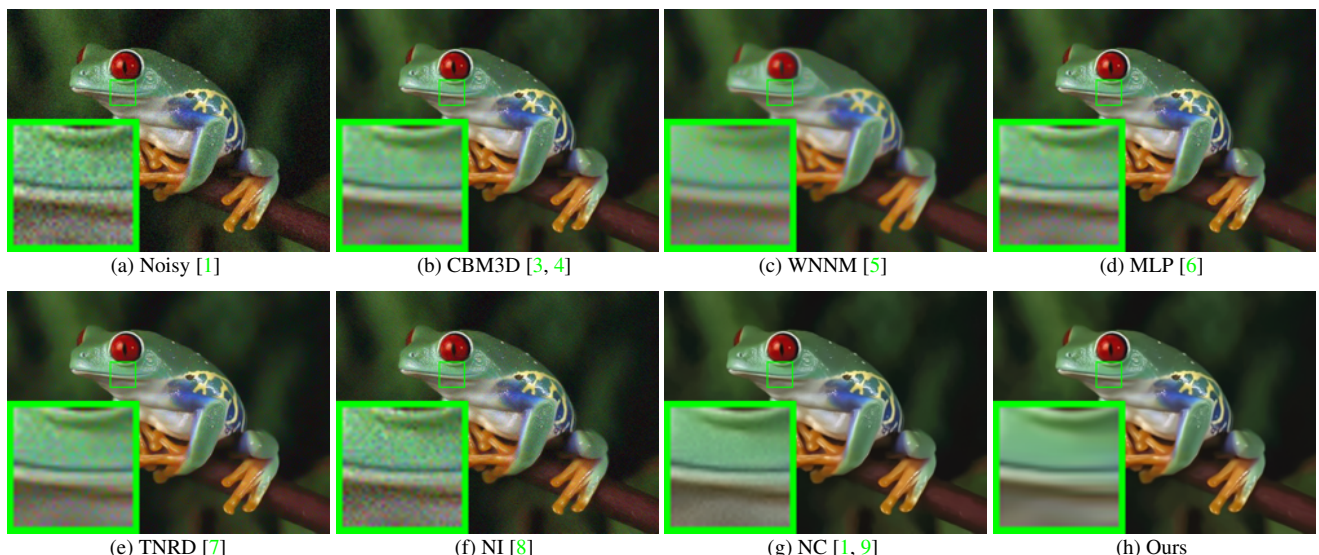
110 In summary, we have the final solution of the weighted sparse coding problem (1) as  
 111

$$\hat{\alpha} = \text{sgn}(\mathbf{D}^T \mathbf{y}) \odot \max(|\mathbf{D}^T \mathbf{y}| - \lambda, 0), \quad (11)$$

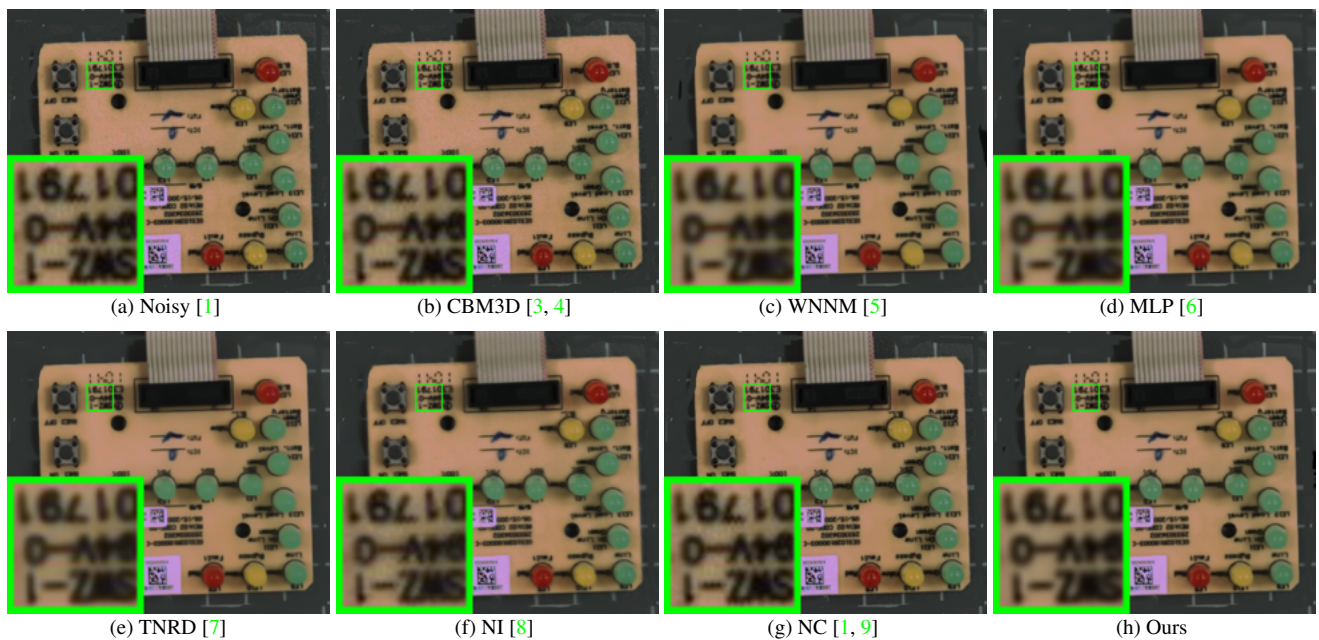
112 where  $\lambda = \frac{1}{2}[\lambda_1, \lambda_2, \dots, \lambda_{3p^2}]^\top$  is the vector of regularization parameter and  $\odot$  means element-wise multiplication.  
 113

## 114 2. More Denoising Results on the Real Noisy Images in Dataset [1]

115 In this section, we give more comparisons of the competing methods on the dataset [1]. The real noisy images in dataset  
 116 [1] have no “ground truth” images and hence we only compare the visual quality of the denoised images by different methods.  
 117 As can be seen from Figures 1-4, our proposed method performs better than the state-of-the-art denoising methods.  
 118



119 Figure 1. Denoised images of the real noisy image “Frog” [1] by different methods. The images are better to be zoomed in on screen.  
 120



121 Figure 2. Denoised images of the real noisy image “Circuit” [1] by different methods. The images are better to be zoomed in on screen.  
 122

216  
217  
218  
219  
220  
221  
222  
223  
224  
225  
226(a) Noisy [1] (b) CBM3D [3, 4] (c) WNNM [5] (d) MLP [6]  
(e) TNRD [7] (f) NI [8] (g) NC [1, 9] (h) Ours227  
228  
229  
230  
231  
232  
233  
234  
235  
236  
237

Figure 3. Denoised images of the real noisy image “Woman” [1] by different methods. The images are better to be zoomed in on screen.

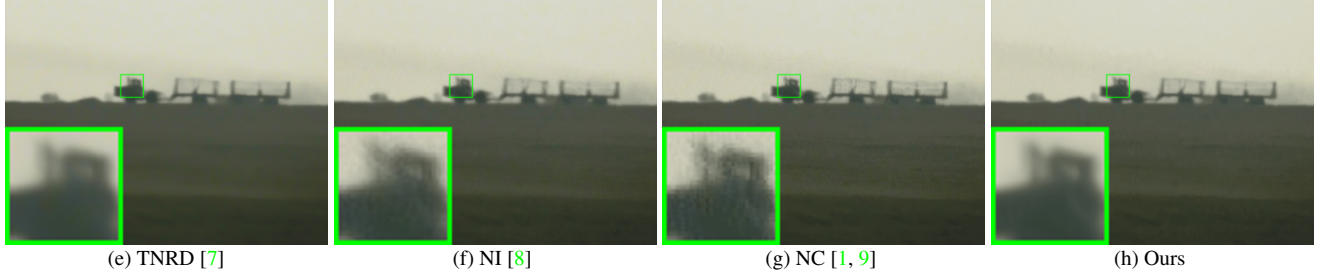
238  
239(a) Noisy [1] (b) CBM3D [3, 4] (c) WNNM [5] (d) MLP [6]  
(e) TNRD [7] (f) NI [8] (g) NC [1, 9] (h) Ours240  
241  
242  
243  
244  
245  
246  
247  
248  
249(a) Noisy [1] (b) CBM3D [3, 4] (c) WNNM [5] (d) MLP [6]  
(e) TNRD [7] (f) NI [8] (g) NC [1, 9] (h) Ours250  
251  
252  
253  
254  
255  
256  
257  
258  
259

Figure 4. Denoised images of the real noisy image “Vehicle” [1] by different methods. The images are better to be zoomed in on screen.

260  
261  
262

### 3. More Denoising Results on the 15 Cropped Images Used in [2]

263  
264  
265  
266  
267  
268  
269

In this section, we provide more visual comparisons of the proposed method with the state-of-the-art denoising methods on the 15 cropped real noisy images used in [2]. In this dataset, each scene was shot 500 times under the same camera and camera setting. The mean image of the 500 shots is roughly taken as the “ground truth”, with which the PSNR can be computed. As can be seen from Figures 5-9, in most cases, our proposed method achieves better performance than the competing methods. This validates the effectiveness of our proposed external prior guided internal prior learning framework for real noisy image denoising.

270  
271  
272  
273  
274  
275  
276  
277  
278  
279  
280  
281  
282  
283  
284  
285  
286  
287  
288  
289  
290  
291  
292  
293  
294  
295  
296  
297  
298  
299  
300  
301  
302  
303  
304  
305  
306  
307  
308  
309  
310  
311  
312  
313  
314  
315  
316  
317  
318  
319  
320  
321  
322  
323

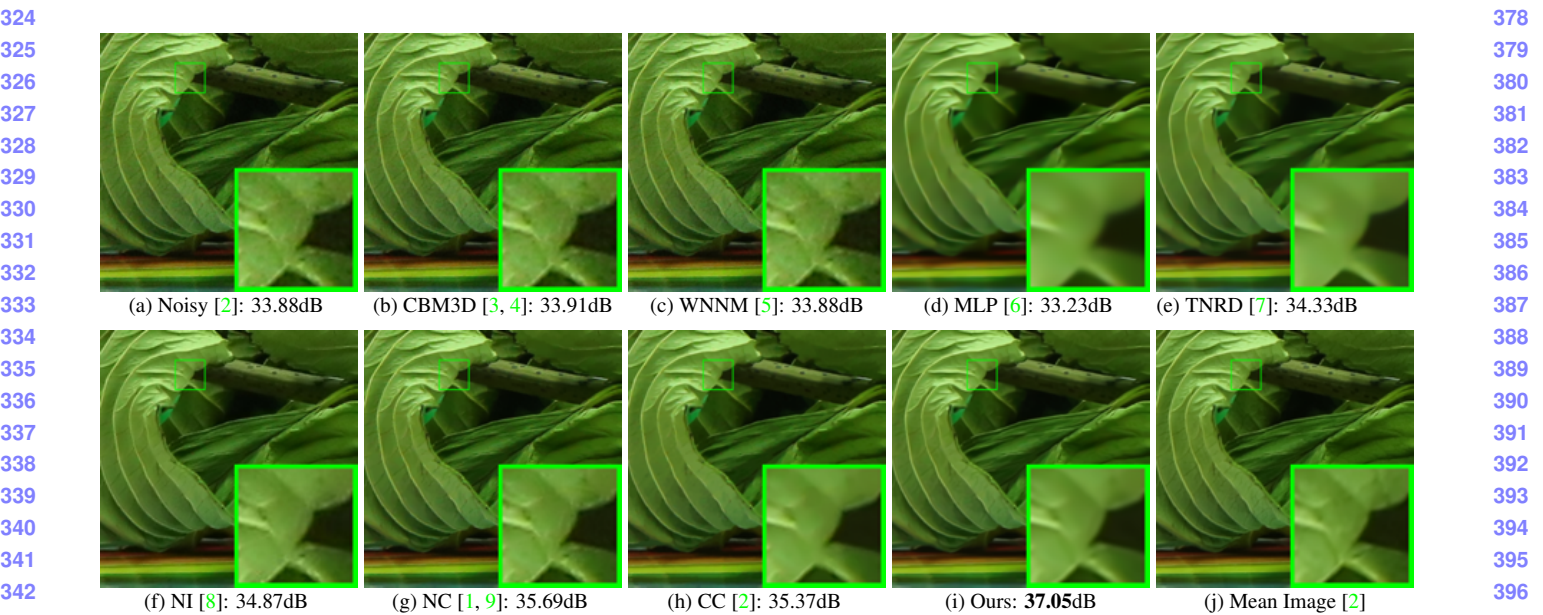


Figure 5. Denoised images of a region cropped from the real noisy image “Canon 5D Mark 3 ISO 3200 2” [2] by different methods. The images are better to be zoomed in on screen.

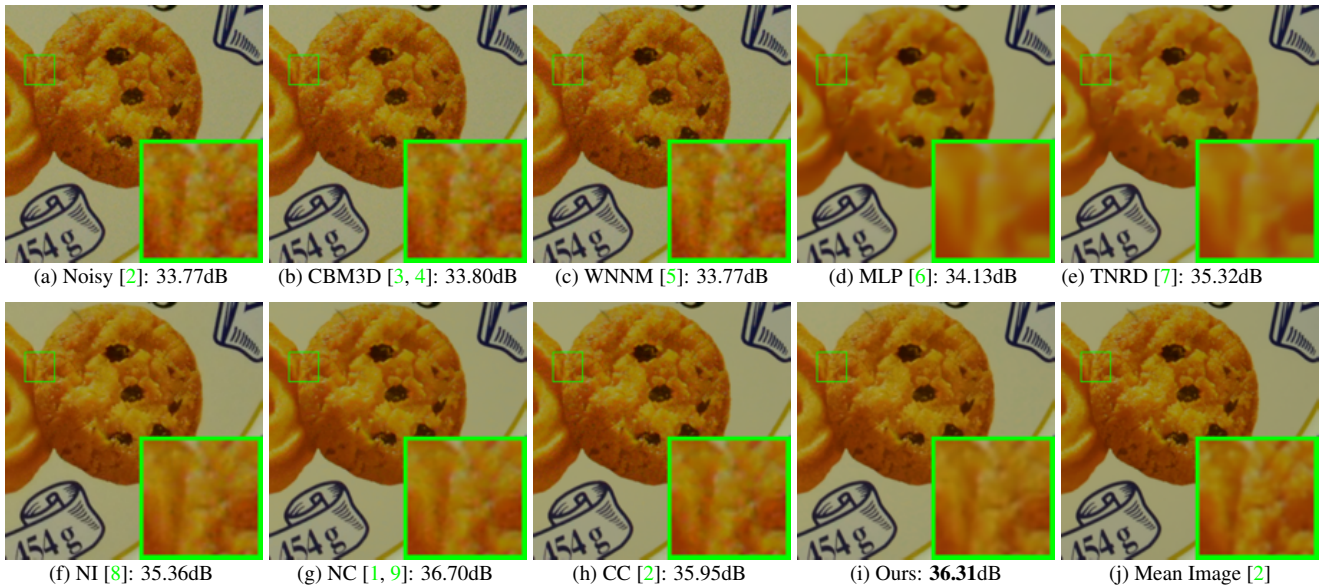


Figure 6. Denoised images of a region cropped from the real noisy image “Canon 5D Mark 3 ISO 3200 2” [2] by different methods. The images are better to be zoomed in on screen.

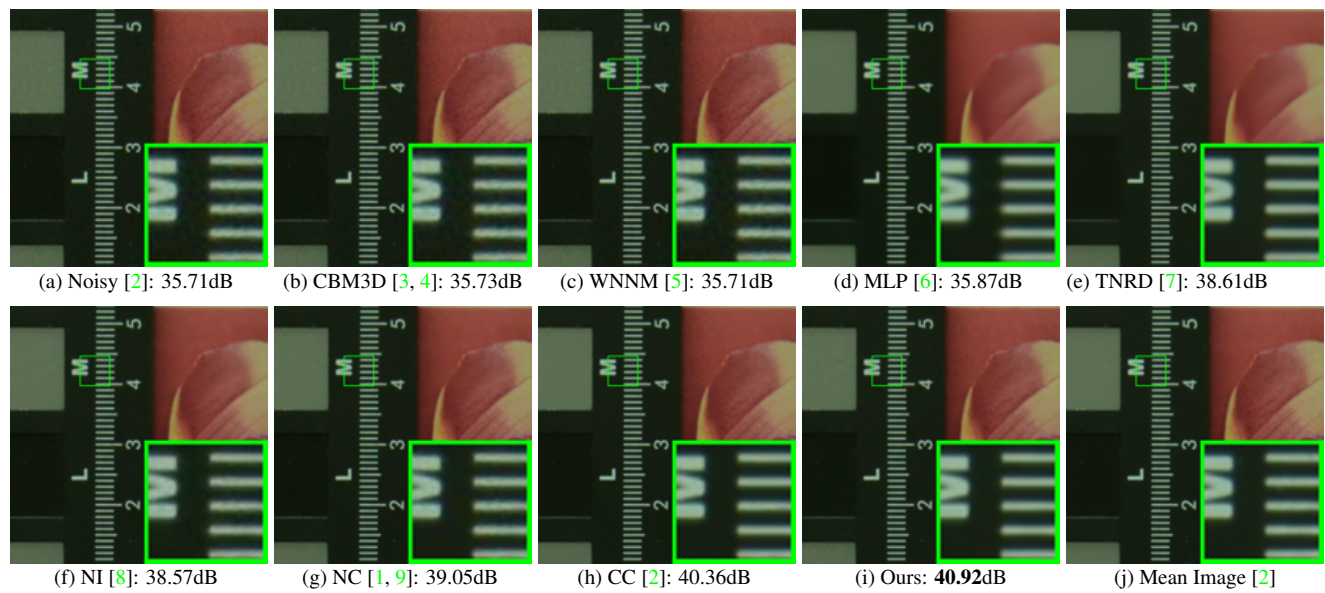


Figure 7. Denoised images of a region cropped from the real noisy image “Nikon D800 ISO 1600 2” [2] by different methods. The images are better to be zoomed in on screen.

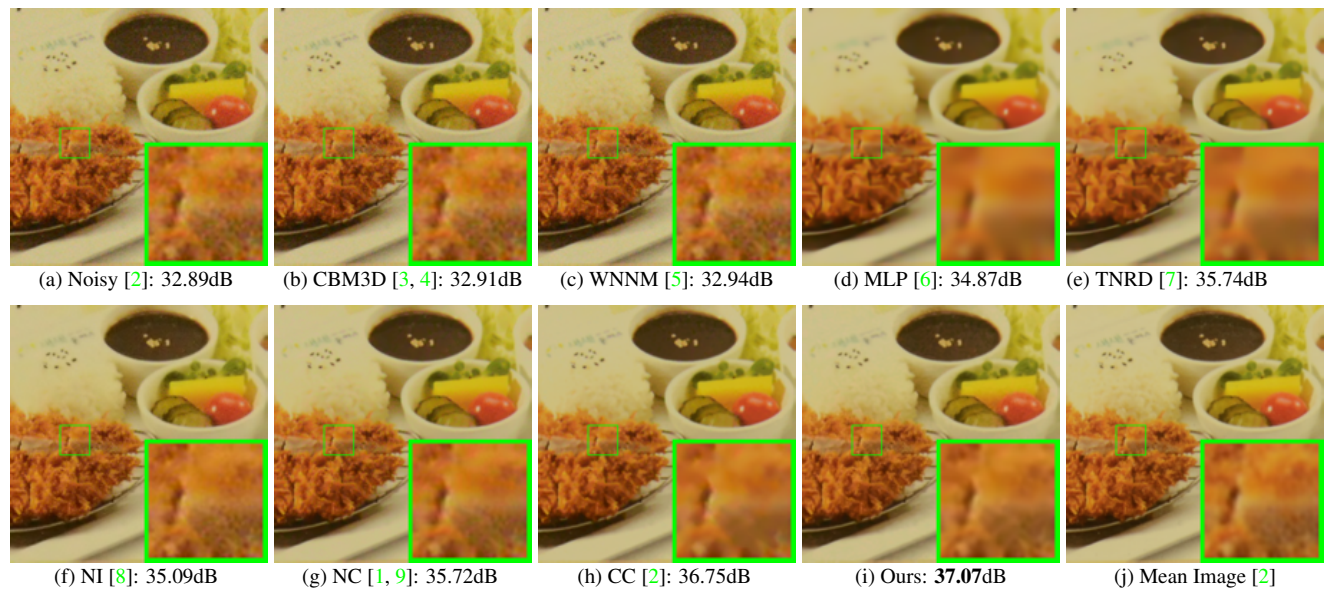


Figure 8. Denoised images of a region cropped from the real noisy image “Nikon D800 ISO 3200 2” [2] by different methods. The images are better to be zoomed in on screen.

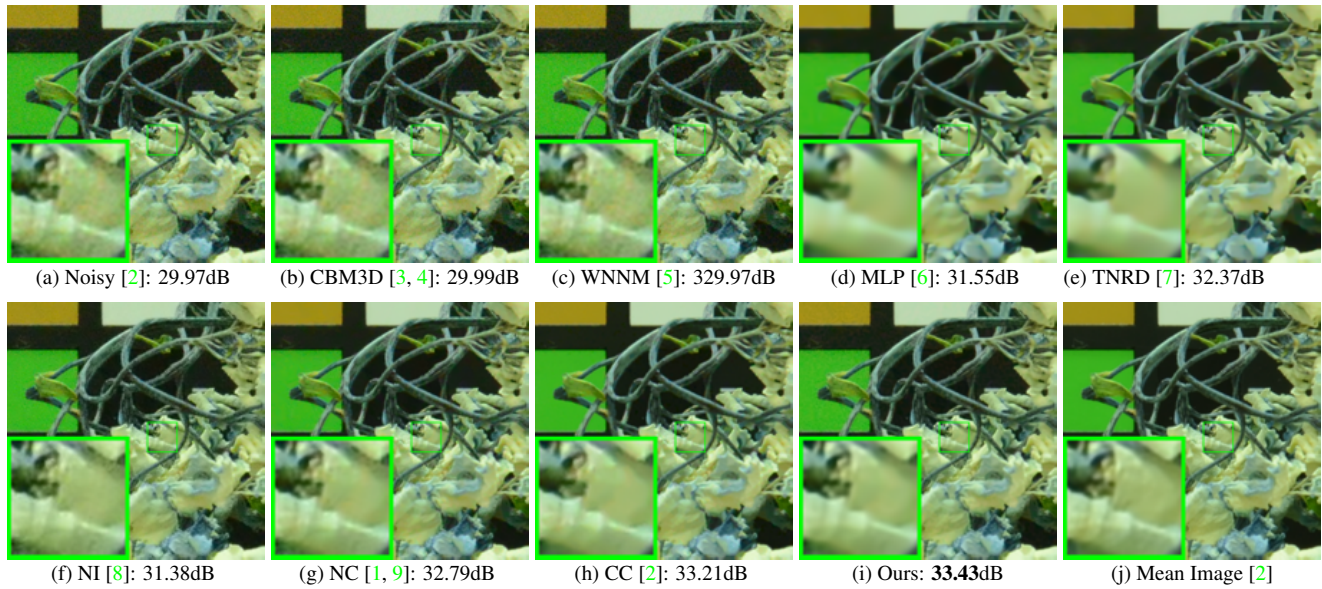


Figure 9. Denoised images of a region cropped from the real noisy image “Nikon D800 ISO 6400 2” [2] by different methods. The images are better to be zoomed in on screen.

#### 4. More Denoising Results on the 60 Cropped Real Noisy Images from [2]

In this section, we provide more visual comparisons of the proposed method with the state-of-the-art denoising methods on the 60 cropped real noisy images we cropped from [2]. In this dataset, each scene was shot 500 times under the same camera and camera setting. The mean image of the 500 shots is roughly taken as the “ground truth”, with which the PSNR can be computed. As can be seen from Figures 10-20, in most cases, our proposed method achieves better performance than the competing methods. This validates the effectiveness of our proposed external prior guided internal prior learning framework for real noisy image denoising.

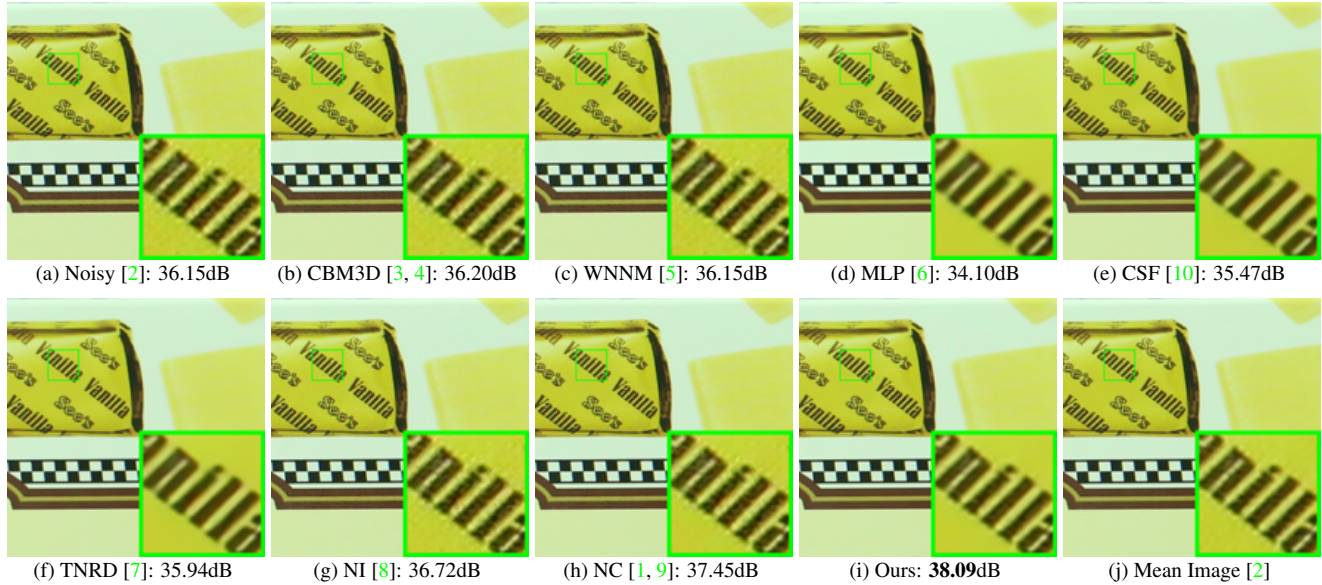


Figure 10. Denoised images of a region cropped from the real noisy image “Canon EOS 5D Mark3 ISO 3200 C1” [2] by different methods. The images are better viewed by zooming in on screen.

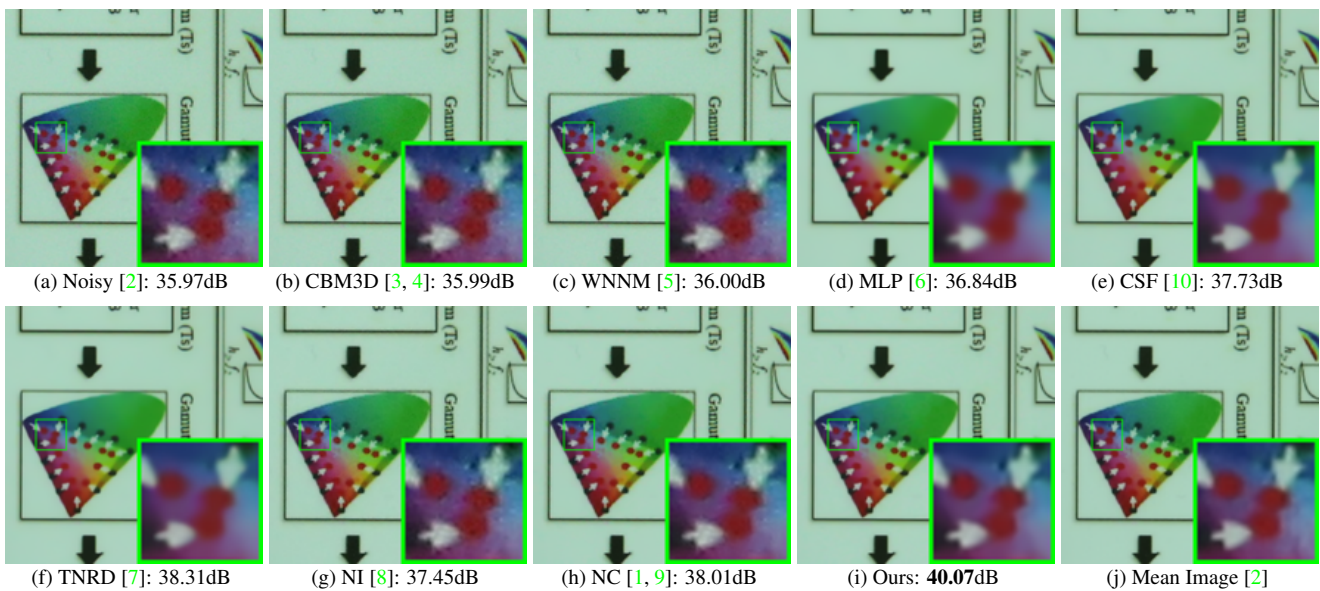


Figure 11. Denoised images of a region cropped from the real noisy image “Canon EOS 5D Mark3 ISO 3200 C2” [2] by different methods. The images are better viewed by zooming in on screen.

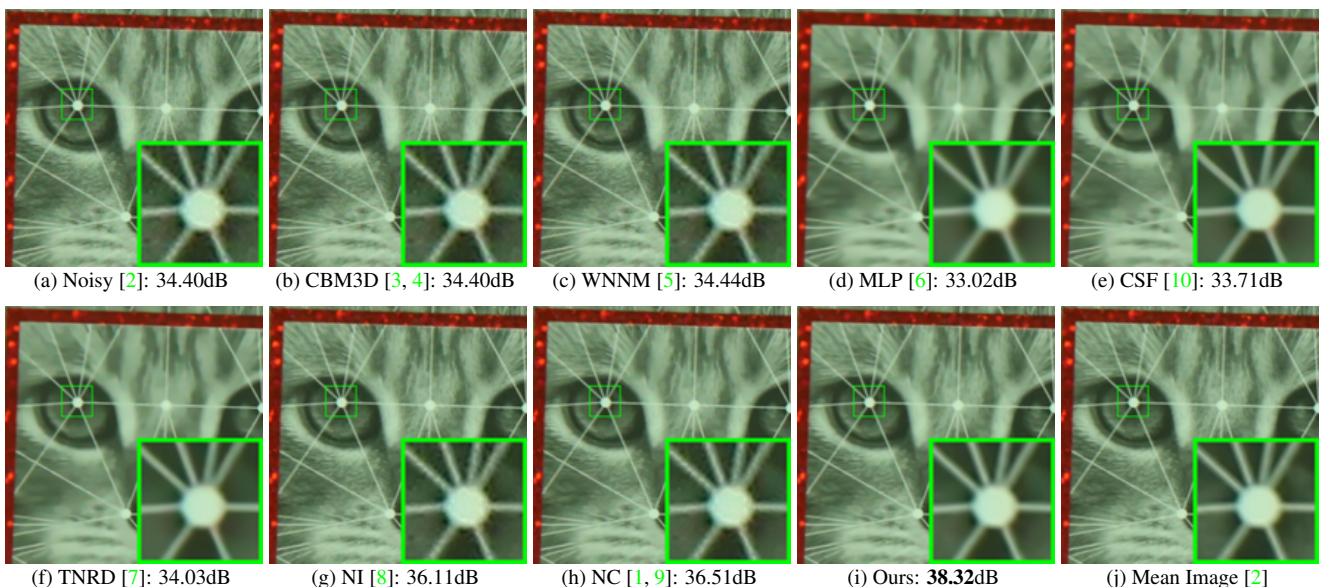


Figure 12. Denoised images of a region cropped from the real noisy image “Canon EOS 5D Mark3 ISO 3200 C3” [2] by different methods. The images are better viewed by zooming in on screen.

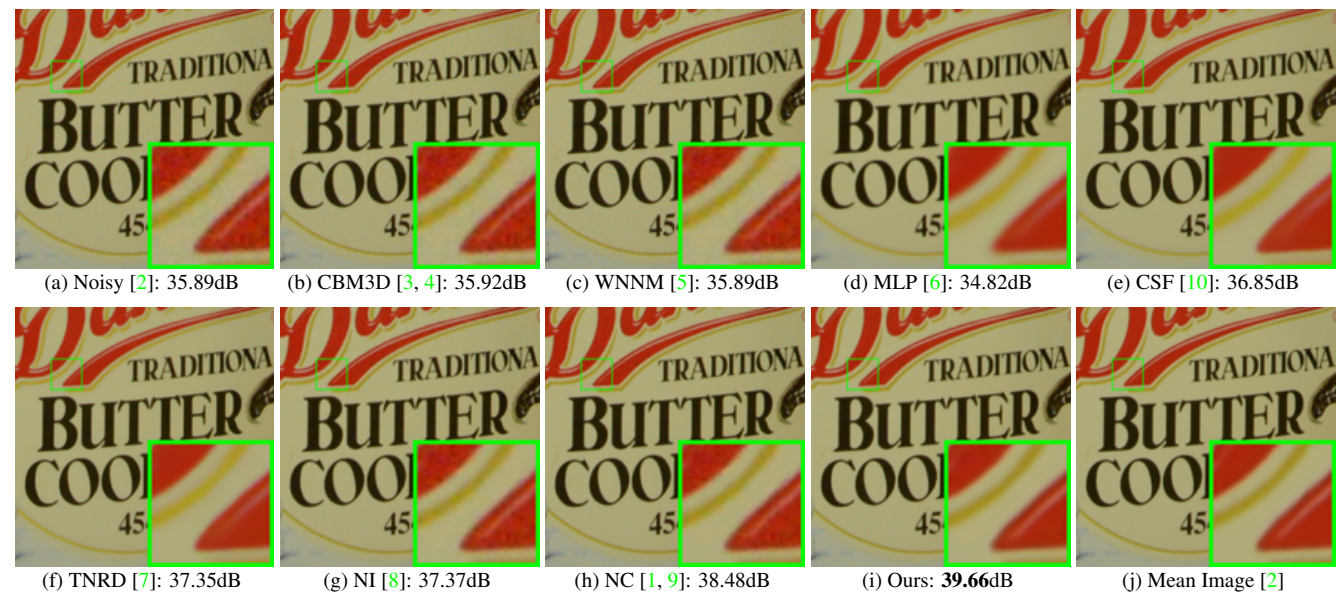


Figure 13. Denoised images of a region cropped from the real noisy image “Nikon D600 ISO 3200 C1” [2] by different methods. The images are better viewed by zooming in on screen.

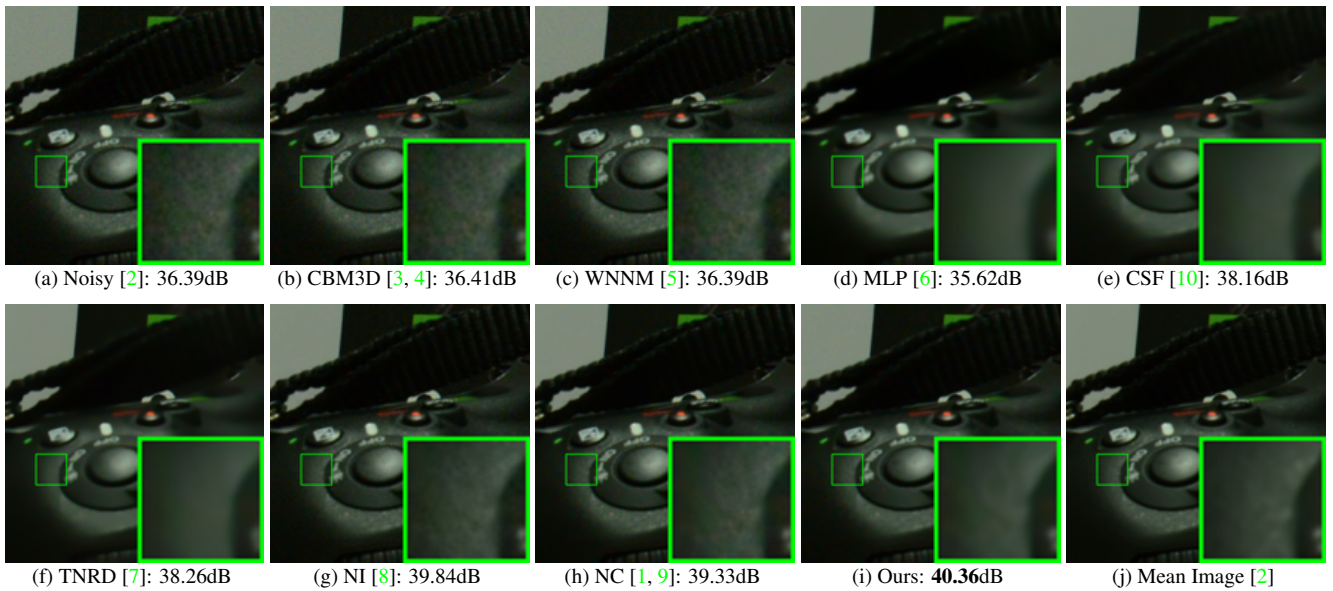


Figure 14. Denoised images of a region cropped from the real noisy image “Nikon D600 ISO 3200 C2” [2] by different methods. The images are better viewed by zooming in on screen.

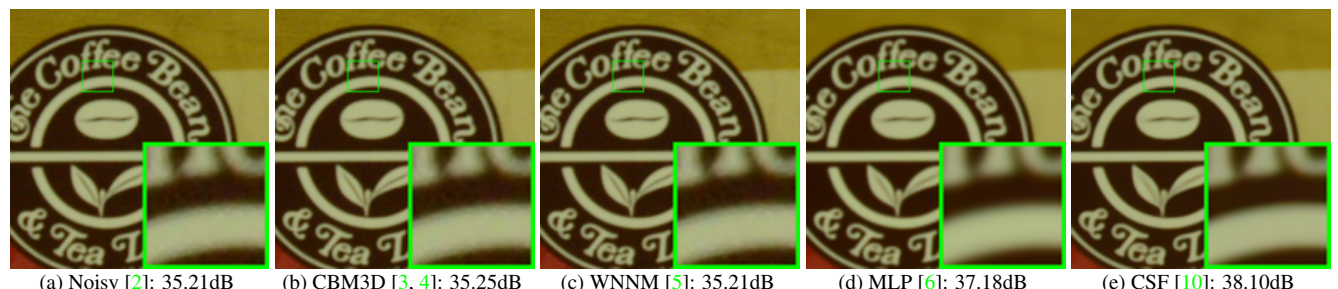


Figure 15. Denoised images of a region cropped from the real noisy image “Nikon D800 ISO 1600 B2” [2] by different methods. The images are better viewed by zooming in on screen.

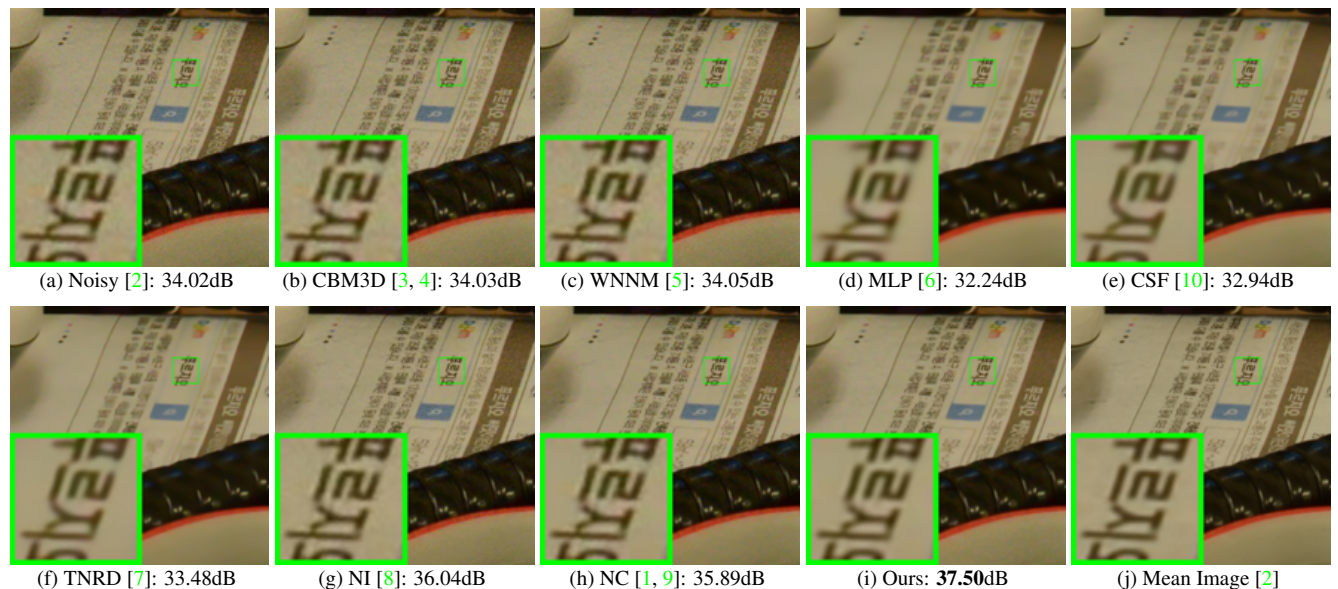


Figure 16. Denoised images of a region cropped from the real noisy image “Nikon D800 ISO 3200 A1” [2] by different methods. The images are better viewed by zooming in on screen.

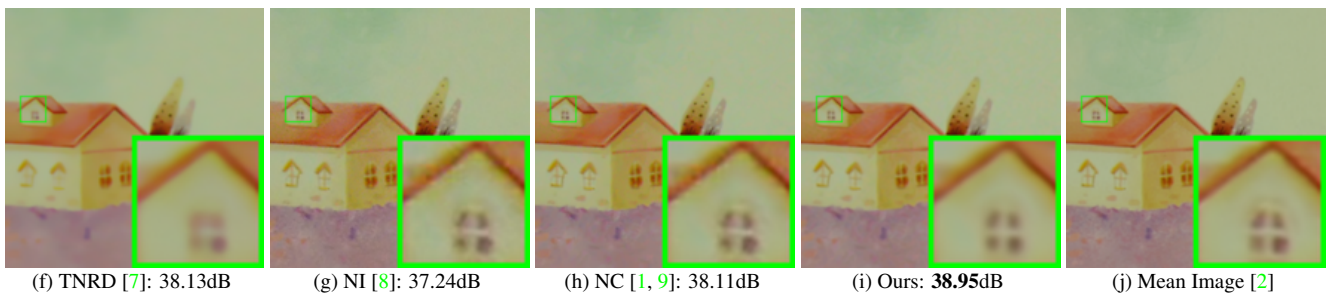
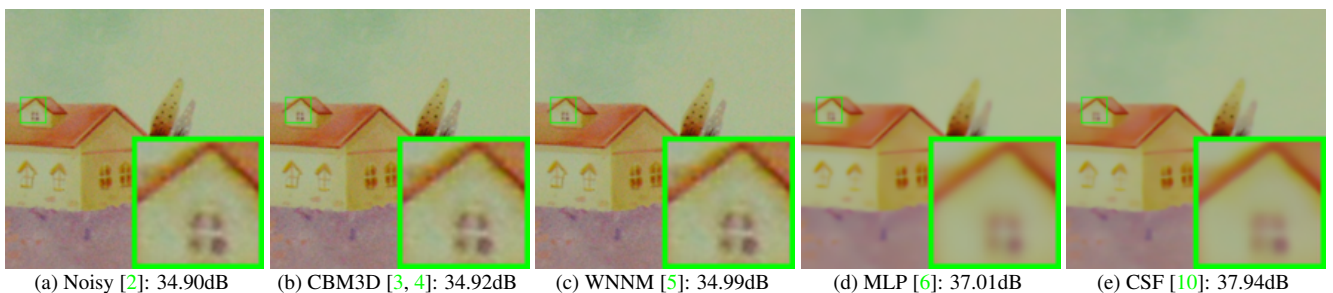


Figure 17. Denoised images of a region cropped from the real noisy image “Nikon D800 ISO 3200 A2” [2] by different methods. The images are better viewed by zooming in on screen.

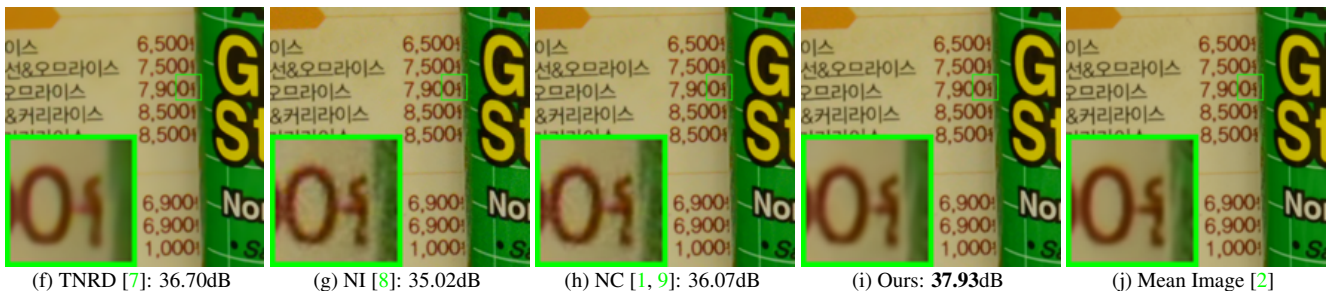
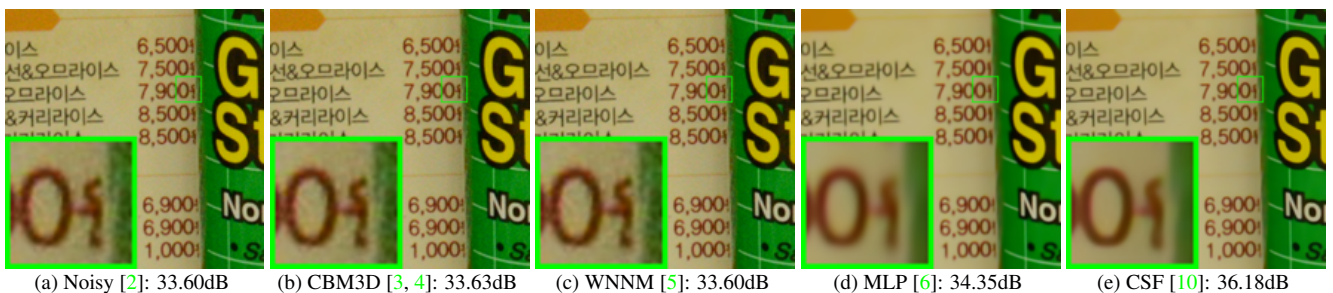


Figure 18. Denoised images of a region cropped from the real noisy image “Nikon D800 ISO 3200 A3” [2] by different methods. The images are better viewed by zooming in on screen.

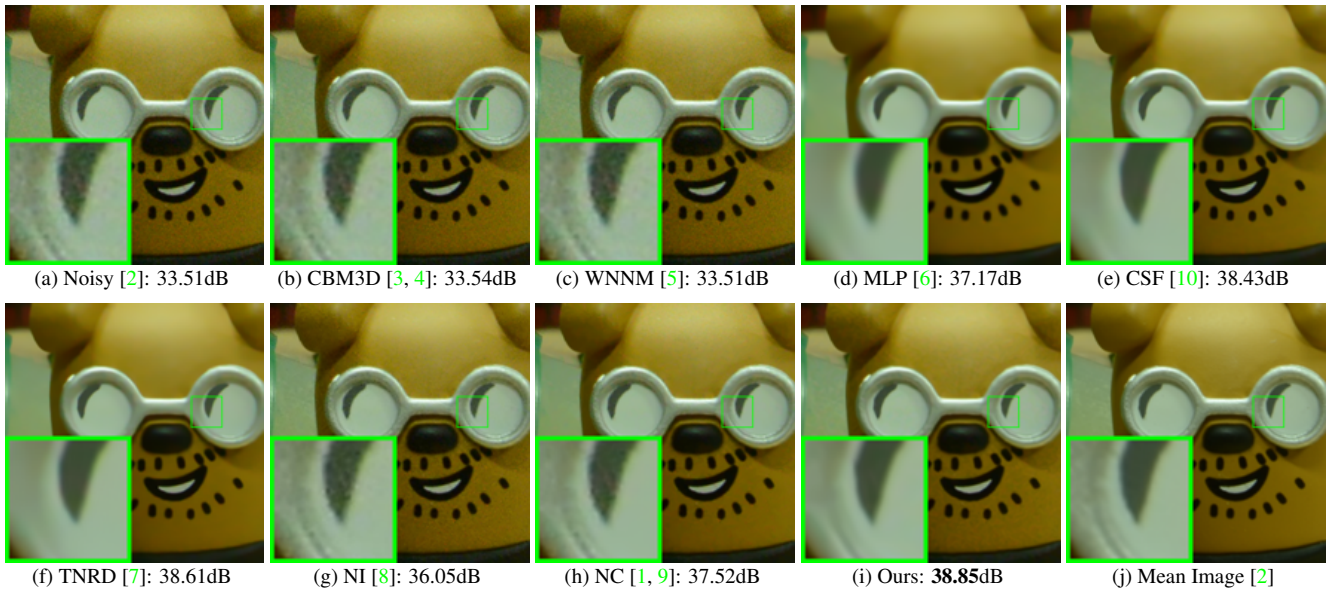


Figure 19. Denoised images of a region cropped from the real noisy image “Nikon D800 ISO 3200 A4” [2] by different methods. The images are better viewed by zooming in on screen.

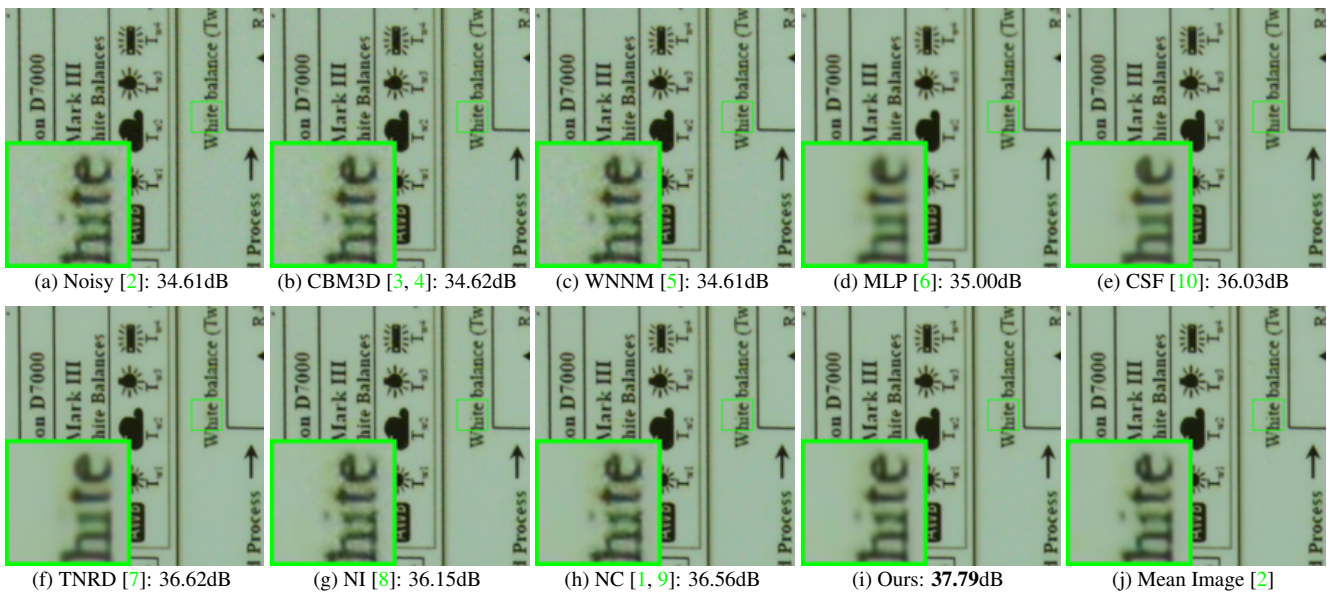


Figure 20. Denoised images of a region cropped from the real noisy image “Nikon D800 ISO 3200 A5” [2] by different methods. The images are better viewed by zooming in on screen.

## References

- [1] M. Lebrun, M. Colom, and J. M. Morel. The noise clinic: a blind image denoising algorithm. <http://www.ipol.im/pub/art/2015/125/>. Accessed 01 28, 2015. 1, 2, 3, 4, 5, 6, 7, 8, 9, 10, 11
- [2] S. Nam, Y. Hwang, Y. Matsushita, and S. J. Kim. A holistic approach to cross-channel image noise modeling and its application to image denoising. *IEEE Conference on Computer Vision and Pattern Recognition (CVPR)*, pages 1683–1691, 2016. 1, 3, 4, 5, 6, 7, 8, 9, 10, 11
- [3] K. Dabov, A. Foi, V. Katkovnik, and K. Egiazarian. Image denoising by sparse 3-D transform-domain collaborative filtering. *IEEE Transactions on Image Processing*, 16(8):2080–2095, 2007. 2, 3, 4, 5, 6, 7, 8, 9, 10, 11

- 1188 [4] K. Dabov, A. Foi, V. Katkovnik, and K. Egiazarian. Color image denoising via sparse 3D collaborative filtering with grouping  
1189 constraint in luminance-chrominance space. *IEEE International Conference on Image Processing (ICIP)*, pages 313–316, 2007. 2, 1242  
1190 3, 4, 5, 6, 7, 8, 9, 10, 11 1243  
1191 [5] S. Gu, L. Zhang, W. Zuo, and X. Feng. Weighted nuclear norm minimization with application to image denoising. *IEEE Conference*  
1192 *on Computer Vision and Pattern Recognition (CVPR)*, pages 2862–2869, 2014. 2, 3, 4, 5, 6, 7, 8, 9, 10, 11 1244  
1193 [6] H. C. Burger, C. J. Schuler, and S. Harmeling. Image denoising: Can plain neural networks compete with BM3D? *IEEE Conference*  
1194 *on Computer Vision and Pattern Recognition (CVPR)*, pages 2392–2399, 2012. 2, 3, 4, 5, 6, 7, 8, 9, 10, 11 1245  
1195 [7] Y. Chen, W. Yu, and T. Pock. On learning optimized reaction diffusion processes for effective image restoration. *IEEE Conference*  
1196 *on Computer Vision and Pattern Recognition (CVPR)*, pages 5261–5269, 2015. 2, 3, 4, 5, 6, 7, 8, 9, 10, 11 1246  
1197 [8] Neatlab ABSoft. Neat Image. <https://ni.neatvideo.com/home>. 2, 3, 4, 5, 6, 7, 8, 9, 10, 11 1247  
1198 [9] M. Lebrun, M. Colom, and J.-M. Morel. Multiscale image blind denoising. *IEEE Transactions on Image Processing*, 24(10):3149–  
1200 3161, 2015. 2, 3, 4, 5, 6, 7, 8, 9, 10, 11 1248  
1201 [10] U. Schmidt and S. Roth. Shrinkage fields for effective image restoration. *IEEE Conference on Computer Vision and Pattern Recog-*  
1202 *nition (CVPR)*, pages 2774–2781, June 2014. 6, 7, 8, 9, 10, 11 1249  
1203  
1204  
1205  
1206  
1207  
1208  
1209  
1210  
1211  
1212  
1213  
1214  
1215  
1216  
1217  
1218  
1219  
1220  
1221  
1222  
1223  
1224  
1225  
1226  
1227  
1228  
1229  
1230  
1231  
1232  
1233  
1234  
1235  
1236  
1237  
1238  
1239  
1240  
1241